Earthquake Engineering & Structural Dynamics
The Journal of the International Association for Earthquake Engineering

EARTHQUAKE ENGINEERING & STRUCTURAL DYNAMICS
Earthquake Engng Struct. Dyn. (2012)
Published online in Wiley Online Library (wileyonlinelibrary.com). DOI: 10.1002/eqe.2222

Planar rocking response and stability analysis of an array of free-standing columns capped with a freely supported rigid beam

Nicos Makris*,† and Michalis F. Vassiliou

Department of Civil Engineering, Division of Structures, University of Patras, Patras, GR-26500, Greece

SUMMARY

This paper investigates the planar rocking response of an array of free-standing columns capped with a freely supported rigid beam in an effort to explain the appreciable seismic stability of ancient free-standing columns that support heavy epistyles together with the even heavier frieze atop. Following a variational formulation, the paper concludes to the remarkable result that the dynamic rocking response of an array of free-standing columns capped with a rigid beam is identical to the rocking response of a single free-standing column with the same slenderness yet with larger size, that is a more stable configuration. Most importantly, the study shows that the heavier the freely supported cap beam is (epistyles with frieze atop), the more stable is the rocking frame regardless of the rise of the center of gravity of the cap beam, concluding that top-heavy rocking frames are more stable than when they are top light. This 'counter intuitive' finding renders rocking isolation a most attractive alternative for the seismic protection of bridges with tall piers, whereas its potential implementation shall remove several of the concerns associated with the seismic connections of prefabricated bridges. Copyright © 2012 John Wiley & Sons, Ltd.

Received 8 January 2012; Revised 23 March 2012; Accepted 23 April 2012

KEY WORDS: rocking frame; seismic isolation; ancient temples; prefabricated bridges; earthquake engineering

1. INTRODUCTION

Under base shaking, slender objects and tall rigid structures may enter into rocking motion that occasionally results in overturning. Early studies on the seismic response of a slender rigid block were presented by Milne [1]; however, it was Housner [2] who uncovered a size-frequency scale effect that explained why (i) the larger of two geometrically similar blocks can survive the excitation that will topple the smaller block and (ii) out of two same acceleration amplitude pulses, the one with the longer duration is more capable to induce overturning. Following Housner's seminal paper, a number of studies have been presented to address the complex dynamics of one of the simplest man-made structures – the free-standing rigid column.

Yim *et al*. [3] conducted numerical studies by adopting a probabilistic approach; Aslam *et al*. [4] confirmed with experimental studies that the rocking response of rigid blocks is sensitive to system parameters, whereas Psycharis and Jennings [5] examined the uplift of rigid bodies supported on viscoelastic foundation. Subsequent studies by Spanos and Koh [6] investigated the rocking response due to harmonic steady-state loading and identified 'safe' and 'unsafe' regions together with the fundamental and suharmonic modes of the system. Their study was extended by Hogan [7, 8] who further elucidated the mathematical structure of the problem by introducing the concepts of orbital

*Correspondence to: Nicos Makris, Department of Civil Engineering, Division of Structures, University of Patras, Patras GR-26500, Greece.
†E-mail: nmakris@upatras.gr

stability and Poincare sections. The transient rocking response of free-standing rigid blocks was examined in depth by Zhang and Makris [9] who showed that there exist two modes of overturning: (i) by exhibiting one or more impacts; and (ii) without exhibiting any impact. The existence of the second mode of overturning results in a safe region that is located on the acceleration-frequency plane above the minimum overturning acceleration spectrum. The fundamental differences between the response of a rocking rigid column (inverted pendulum) and the response of the linear elastic oscillator (regular pendulum) led to the development of the rocking spectrum [10]. More recent studies pertinent to the rocking response of rigid columns have focused on more practical issues such as representation of the impact [11], the effect of the flexibility yielding of the supporting base [12, 13], or the effect of seismic isolation [14].

In this paper, we investigate the planar rocking response of an array of free-standing columns capped with a freely supported rigid beam as shown schematically in Figure 1. Herein, we use the term 'rocking frame' for the single DOF structure shown in Figure 1. Sliding does not occur at the pivot points either at the base or at the cap beam.

Our interest to this problem was partly motivated from the need to explain the remarkable seismic stability of ancient free-standing columns that support heavy free-standing epistyles together with the even heavier frieze atop. As an example, Figure 2 shows the entrance view of the late archaic Temple of Aphaia in the island of Aegina nearby Athens, Greece. Dates ranging from 510 BC to 470 BC have been proposed for this temple. All but three of the 32 outer columns of the temple are monolithic, and they have been supporting for 2.5 millennia the front and back epistyles together with the heavy frieze (triglyph and metope). Figure 3 shows the monolithic free-standing columns of the Temple of Apollo in Corinth, Greece, either standing alone or supporting epistyles, which have survived toppling, in an area with high seismicity, since 540 BC. In ancient Greek temples, the epistyles are positioned from the vertical axis of one column to the vertical axis of the neighboring column; therefore, the joint of the epistyles are along the vertical axis of the column (see Figure 2). With this configuration during lateral loading of the peristyle of the temple, each epistyle in addition to the horizontal translation, u, shown in Figure 1 will also experience a small rotation, whereas the transfer of forces from the epistyles to the columns is not concentrated at the top pivoting point of the columns. Accordingly, the planar rocking response of the peristyle of ancient temples is more complicated than the planar motion of the idealization shown in Figure 1.

Nevertheless, the striking dynamic stability of these monuments is mainly due to the development of rocking mechanisms. Motivated from this outstanding performance, this paper examines the dynamic response and stability of the simplest free-standing rocking frame shown in Figure 1 in an effort to improve our understanding regarding the dynamics of this class of nonlinear articulated structures.

The understanding of the rocking response and stability of the configuration shown in Figure 1 is also pertinent to the growing precast bridge construction technology where bridge piers supporting heavy decks are allowed to rock atop their foundation to achieve re-centering of the bridge bent after a seismic event.

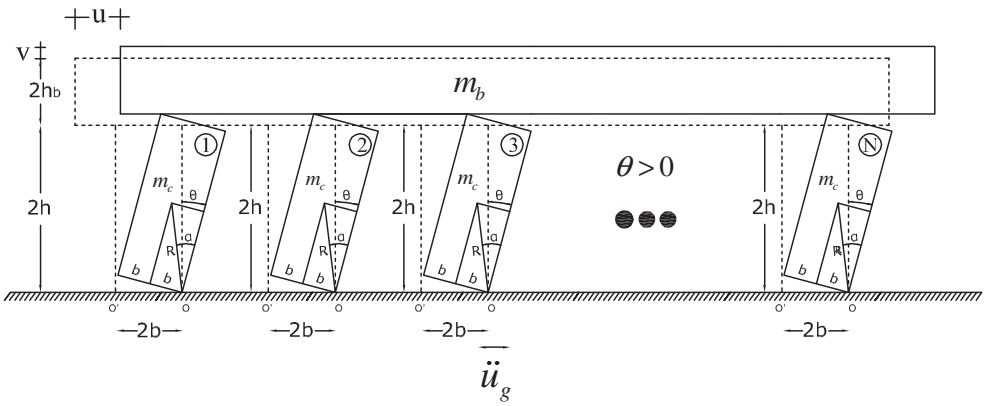

Figure 1. Rocking array of free-standing columns capped with a freely supported rigid beam.

DOI: 10.1002/eqe

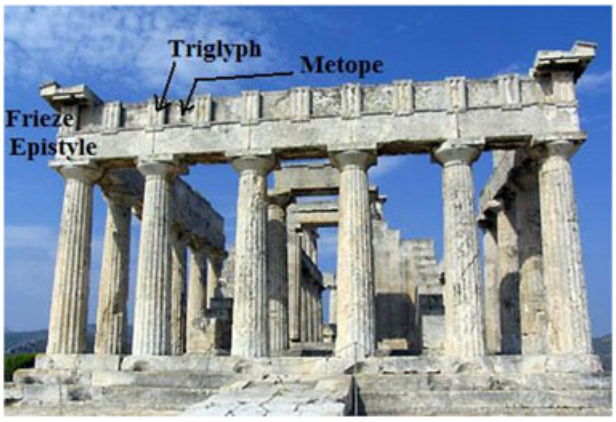

Figure 2. View of the Temple of Aphaia, in Aegina, Greece. Its monolithic, free-standing columns support massive epistyles and the frieze atop, and the entire rocking frame remains standing for more than 2500 years in a region with high seismicity.

Figure 3. View of the Temple of Apollo, in Corinth, Greece. Its monolithic, free-standing columns support massive epistyles and remain standing in an area of high seismicity since 540 BC.

2. REVIEW OF THE ROCKING RESPONSE OF A FREE-STANDING RIGID COLUMN

With reference to Figure 4 and assuming that the coefficient of friction is large enough so that there is no sliding, the equation of motion of a free-standing block with size $R = \sqrt{h^2 + b^2}$ and slenderness $\alpha = \text{atan}(b/h)$ subjected to a horizontal ground acceleration, $\ddot{u}_g(t)$, when rocking around O and O′, respectively, is ([3, 7, 15, 9] among others)

$$I_o\ddot{\theta}(t) + mgR\sin[\text{-}\alpha\text{-}\theta(t)] = \text{-}m\ddot{u}_g(t)R\cos[\text{-}\alpha\text{-}\theta(t)], \quad \theta(t) < 0 \tag{1}$$

$$I_o\ddot{\theta}(t) + mgR\sin[\alpha\text{-}\theta(t)] = \text{-}m\ddot{u}_g(t)R\cos[\alpha\text{-}\theta(t)], \quad \theta(t) > 0. \tag{2}$$

For rocking motion to be initiated, $\ddot{u}_g(t) > g\tan\alpha$ at some time of its history. For rectangular blocks, $I_o = (4/3)mR^2$; and the aforementioned equations can be expressed in the compact form

$$\ddot{\theta}(t) = -p^2\left\{\sin[\alpha\,\text{sgn}(\theta(t)) - \theta(t)] + \frac{\ddot{u}_g}{g}\cos[\alpha\,\text{sgn}(\theta(t)) - \theta(t)]\right\}. \tag{3}$$

DOI: 10.1002/eqe

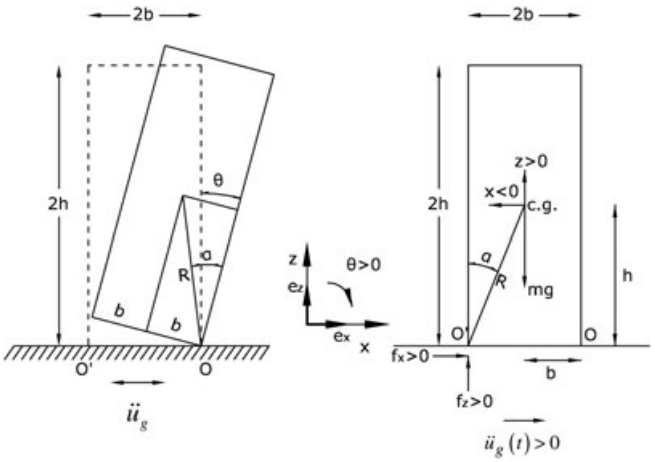

Figure 4. Left: geometric characteristics of the model considered. Right: free-body diagram of a free-standing block at the instant that it enters rocking motion.

The oscillation frequency of a rigid block under free vibration is not constant because it strongly depends on the vibration amplitude [2]. Nevertheless, the quantity $p = \sqrt{3g/4R}$ is a measure of the dynamic characteristics of the block. For the $7.5\,\text{m} \times 1.8\,\text{m}$ free-standing column of the Temple of Appolo in Corinth, $p = 1.4$ rad/s, and for a household brick, $p \approx 8$ rad/s.

Figure 5 shows the moment–rotation relationship during the rocking motion of a free-standing block. The system has infinite stiffness until the magnitude of the applied moment reaches the value $mgR\sin\alpha$, and once the block is rocking, its restoring force decreases monotonically, reaching zero when $\theta = \alpha$. This negative stiffness, which is inherent in rocking systems, is most attractive in earthquake engineering given that such systems do not resonate.

During the oscillatory rocking motion of a free-standing rigid column, the moment–rotation curve follows the curve shown in Figure 5 without enclosing any area. Energy is lost only during impact, when the angle of rotation reverses. When the angle of rotation reverses, it is assumed that the rotation continues smoothly from points O to O' and that the impact force is concentrated at the new pivot point, O'. With this idealization, the impact force applies no moment around O'; hence, the angular momentum around O' is conserved. Conservation of angular momentum about point O' just before the impact and right after the impact gives

$$I_o\dot{\theta}_1 - m\dot{\theta}_1 2bR\sin(\alpha) = I_o\dot{\theta}_2 \tag{4}$$

where $\dot{\theta}_1$ = angular velocity just prior to the impact and $\dot{\theta}_2$ = angular velocity right after the impact. The ratio of kinetic energy after and before the impact is

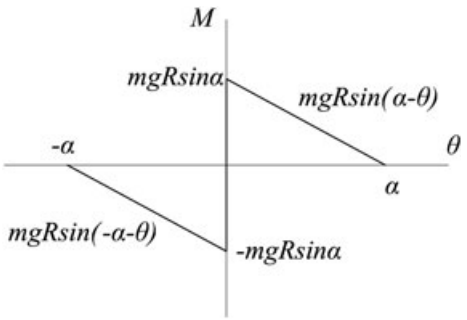

Figure 5. Moment–rotation diagram of a rocking object.

DOI: 10.1002/eqe

$$r = \frac{\dot{\theta}_2^2}{\dot{\theta}_1^2} \tag{5}$$

which means that the angular velocity after the impact is only $\sqrt{r}$ times the velocity before the impact. Substitution of equation (4) into equation (5) gives

$$r = \left[1 - \frac{3}{2}\sin^2\alpha\right]^2 \tag{6}$$

The value of the coefficient of restitution given by equation (6) is the maximum value of r under which a free-standing rigid block with slenderness α will undergo rocking motion. Consequently, to observe rocking motion, the impact has to be inelastic. The less slender a block (larger α), the more plastic is the impact, and for the value of $\alpha = \sin^{-1}\sqrt{2/3} = 54.73^\circ$, the impact is perfectly plastic. During the rocking motion of slender blocks, if additional energy is lost because of the inelastic behavior at the instant of impact, the value of the true coefficient of restitution r will be less than the one computed from equation (6).

3. EQUATION OF MOTION OF THE ROCKING FRAME

The free-standing rocking frame shown in Figure 1 is a single DOF structure with size $R = \sqrt{h^2 + b^2}$ and slenderness $\alpha = a\tan(b/h)$. The only other parameter that influences the dynamics of the rocking frame is the ratio of the mass of the cap beam, m_b, to the mass of all the N rocking columns, m_c, $\gamma = m_b/Nm_c$. For the Temple of Apollo in Corinth where the frieze is missing, γ is as low as 0.3, whereas in prefabricated bridges, $\gamma > 4$. As in the case of the single rocking column, the coefficient of friction is large enough so that sliding does not occur at the pivot point at the base and at the cap beam. Accordingly, the horizontal translation displacement $u(t)$ and the vertical lift $v(t)$ of the cap beam are functions of the single DOF $\theta(t)$. For a positive horizontal ground acceleration (the ground is accelerating to the right), the rocking frame will initially rock to the left ($\theta(t) < 0$). Assuming that the rocking frame will not topple, it will re-center, impacts will happen at the pivot points (at the base and at the cap beam), and subsequently, it will rock to the right ($\theta(t) > 0$). During rocking, the dependent variables $u(t)$, $v(t)$ and their time derivatives are given for $\theta(t) < 0$ and $\theta(t) > 0$ by the following expressions.

$$u = 2R(\sin\alpha - \sin(\alpha \pm \theta)) \tag{7}$$

$$\dot{u} = \mp 2R\cos(\alpha \pm \theta)\dot{\theta} \tag{8}$$

$$\ddot{u} = 2R\left(\sin(\alpha \pm \theta)\left(\dot{\theta}\right)^2 - \cos(\alpha \pm \theta)\ddot{\theta}\right) \tag{9}$$

and

$$v = 2R(\cos(\alpha \pm \theta) - \cos\alpha) \tag{10}$$

$$\dot{v} = \mp 2R\sin(\alpha \pm \theta)\dot{\theta} \tag{11}$$

$$\ddot{v} = 2R\left(-\cos(\alpha \pm \theta)\left(\dot{\theta}\right)^2 \mp \sin(\alpha \pm \theta)\ddot{\theta}\right) \tag{12}$$

In these equations, whenever there is a double sign (say $\pm$), the top sign is for $\theta(t) < 0$, and the bottom sign is for $\theta(t) > 0$.

DOI: 10.1002/eqe

During rocking motion, Langrange's equation must be satisfied;

$$\frac{\mathrm{d}}{\mathrm{d}t}\left(\frac{\mathrm{d}T}{\mathrm{d}\dot{\theta}}\right) - \frac{\mathrm{d}T}{\mathrm{d}\theta} = Q. \tag{13}$$

In equation (13), T is the kinetic energy of the system, and Q is the generalized force acting on the system

$$Q = \frac{\mathrm{d}W}{\mathrm{d}\theta} \tag{14}$$

in which W is the work performed by the external forces acting on the rocking frame during an admissible rotation $\delta\theta$. During this admissible rotation $\delta\theta$, the variation of work is

$$\delta W = \frac{dW}{d\theta}\delta\theta \tag{15}$$

In either case where $\theta(t) < 0$ or $\theta(t) > 0$, the kinetic energy of the system is

$$T = N\frac{1}{2}I_o\left(\dot{\theta}\right)^2 + \frac{1}{2}m_b\left((\dot{u})^2 + (\dot{v})^2\right) \tag{16}$$

With the use of equations (8) and (11), equation (16) reduces to

$$T = \left(\frac{N}{2}I_o + 2m_bR^2\right)\left(\dot{\theta}\right)^2 \tag{17}$$

Our analysis proceeds by first investigating the rocking motion of a free-standing frame subjected to a horizontal ground acceleration $\ddot{u}_g(t)$ when $\theta(t) < 0$. During this segment of the motion, the variation of the work, W, is

$$\delta W = \left(m_b + \frac{N}{2}m_c\right)\left(\ddot{u}_g\delta u - g\delta v\right) \tag{18}$$

or

$$\delta W = \left(m_b + \frac{N}{2}m_c\right)\left(\ddot{u}_g\frac{du}{d\theta} - g\frac{dv}{d\theta}\right)\delta\theta \tag{19}$$

The combination of equations (15) and (19) gives

$$\frac{dW}{d\theta} = \left(m_b + \frac{N}{2}m_c\right)\left(\ddot{u}_g\frac{du}{d\theta} - g\frac{dv}{d\theta}\right) \tag{20}$$

which simplifies to

$$\frac{dW}{d\theta} = 2R\left(m_b + \frac{N}{2}m_c\right)\left(-\ddot{u}_g\cos(\alpha+\theta) + g\sin(\alpha+\theta)\right), \tag{21}$$

after using the expression given by equations (7) and (10).

DOI: 10.1002/eqe

The substitution of equations (17) and (21) into Lagrange's equation given by equation (13) results to the equation of motion of the rocking frame for $\theta(t) < 0$.

$$\left(\frac{\frac{I_o}{2m_cR} + 2\gamma R}{\left(\gamma + \frac{1}{2}\right)g}\right)\ddot{\theta} = \sin(a + \theta) - \frac{\ddot{u}_g}{g}\cos(\alpha + \theta), \tag{22}$$

where $\gamma = m_b/Nm_c$ is the ratio of the mass of the cap beam (epistyle), m_b, to the mass of all the N columns $= Nm_c$.

For the case where the rotation is positive $\theta(t) > 0$, the variation of the work is

$$\delta W = -\left(m_b + \frac{N}{m_c}m_c\right)\left(\ddot{u}_g\delta u + g\delta v\right) \tag{23}$$

and equation (14) takes the form

$$\frac{\mathrm{d}W}{\mathrm{d}\theta} = -2R\left(m_b + \frac{N}{2}m_c\right)\left(\ddot{u}_g\cos(\alpha + \theta) + g\sin(\alpha + \theta)\right). \tag{24}$$

The substitution of equations (17) and (24) into Lagrange's equation given by equation (13) offers the equation of motion of the rocking frame for $\theta(t) > 0$.

$$\left(\frac{\frac{I_o}{2m_cR} + 2\gamma R}{\left(\gamma + \frac{1}{2}\right)g}\right)\ddot{\theta} = -\sin(a - \theta) - \frac{\ddot{u}_g}{g}\cos(\alpha - \theta). \tag{25}$$

For rectangular columns, $I_o = (4/3)mR^2$, and equations (22) and (25) can be expressed in a single compact form

$$\ddot{\theta} = -\frac{1 + 2\gamma}{1 + 3\gamma}p^2\left(\sin[a\,\mathrm{sgn}(\theta(t)) - \theta(t)] + \frac{\ddot{u}_g(t)}{g}\cos[a\,\mathrm{sgn}(\theta(t)) - \theta(t)]\right) \tag{26}$$

Equation (26), which describes the planar motion of the free-standing rocking frame, is precisely the same as equation (3), which describes the planar rocking motion of a single free-standing rigid column with the same slenderness α, except that in the rocking frame, the term p^2 is multiplied with the factor $(1 + 2\gamma)/(1 + 3\gamma)$. Accordingly, the frequency parameter of the rocking frame, $\hat{p}$, is

$$\hat{p} = \sqrt{\frac{1 + 2\gamma}{1 + 3\gamma}}p \tag{27}$$

where $p = \sqrt{3g/4R}$ is the frequency parameter of the solitary rocking column and $\gamma = m_b/Nm_c$ is the mass of the cap beam to the mass of all N columns.

For a light cap beam ($\gamma = m_b/Nm_c \to 0$), the multiplication factor $1 + 2\gamma/(1 + 3\gamma) \to 1$ and the array of free-standing columns coupled with a light epistyle exhibit precisely the dynamic rocking response of the solitary free-standing column. On the other hand, as the mass of the epistyle increases,

$$\lim_{\gamma\to\infty}\frac{1 + 2\gamma}{1 + 3\gamma} = \frac{2}{3} \tag{28}$$

Accordingly, the dynamic behavior of a rocking frame with a very heavy cap beam supported on columns with slenderness α and frequency parameter, $p = \sqrt{3g/4R}$, is identical to the dynamic

DOI: 10.1002/eqe

rocking response of a single rigid column with slenderness α and frequency parameter $\hat{p} = \sqrt{2/3}p$ – that is a smaller frequency parameter; therefore a larger, more stable column.

This remarkable result offered by equation (26) – that the heavier the cap beam is, the more stable is the free-standing rocking frame despite the rise of the center of gravity of the cap beam – has been also confirmed by obtaining equation (26) for a pair of columns with the algebraically intense direct formulation after deriving the equations of motion of the two-column frame through dynamic equilibrium. Furthermore, numerical studies with the discrete element method by Papaloizou and Komodromos [16] concluded to the same result – that the planar response of free-standing columns supporting epistyles is more stable than the response of the solitary, free-standing column.

According to equation (26), the rocking response and stability analysis of the free-standing rocking frame with columns having slenderness, α, and size, R, is described by all the past published work on the rocking response of the free-standing single block ([2–4, 6, 9, 10, 14] among others), where the block has the same slenderness, α, and a larger size $\hat{R}$given by

$$\hat{R} = \frac{1+3\gamma}{1+2\gamma}R = \left(1 + \frac{\gamma}{1+2\gamma}\right)R \tag{29}$$

Figure 6 plots the value of $\hat{R}$ as a function of the mass ratio $\gamma = m_b/Nm_c$. When replacing the rocking frame with the larger size, equal slenderness solitary column, the maximum coefficient of restitution is given by equation (43) presented in a later section.

4. MINIMUM ACCELERATION NEEDED TO INITIATE UPLIFT OF A ROCKING FRAME

With reference to Figure 1 during an admissible rotation $\delta\theta$, the application of the principle of virtual work gives

$$m_b\ddot{u}_g\delta u + Nm_c\ddot{u}_gR(\cos\alpha)\delta\theta = m_bg\delta v + Nm_cgR(\sin\alpha)\delta\theta \tag{30}$$

where

$$\delta u = \frac{du}{d\theta}\delta\theta \;\; and \;\; \delta v = \frac{dv}{d\theta}\delta\theta \tag{31}$$

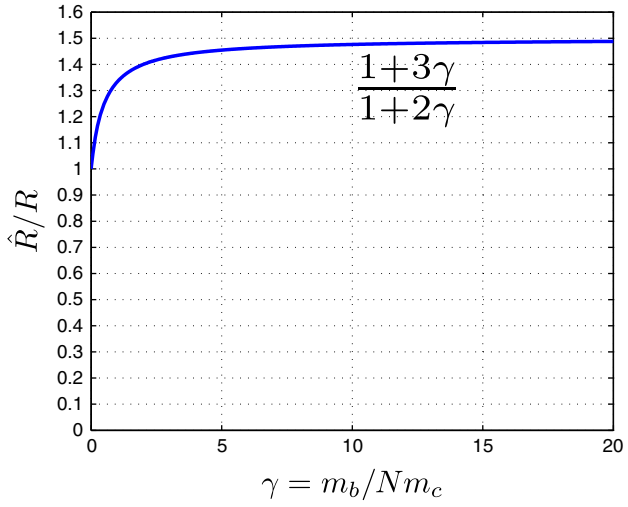

Figure 6. Values of the semidiagonal $\hat{R}$ of a free-standing rigid column with slenderness α that has identical dynamic properties and response as the free-standing rocking frame with N columns having slenderness α, semidiagonal R, and mass m_c, supporting a cap beam with mass m_b.

DOI: 10.1002/eqe

Without loss of generality, we assume that the rocking frame undergoes positive rotations ($\theta(t) > 0$); and according to equations (7) and (10) with their bottom signs,

$$\delta u = 2R\cos(\alpha - \theta)\delta\theta \tag{32}$$

$$\delta v = 2R\sin(\alpha - \theta)\delta\theta \tag{33}$$

Substitution of equations (32) and (33) into equation (30) and after canceling the admissible rotation $\delta\theta$, one obtains

$$m_b\ddot{u}_g 2\cos(\alpha - \theta) + Nm_c\ddot{u}_g\cos\alpha = m_b g 2\sin(\alpha - \theta) + Nm_c g\sin\alpha \tag{34}$$

At the initiation of uplift, $\theta = 0$, and equation (34) simplifies to

$$(2m_b + Nm_c)\ddot{u}_g^{up}\cos\alpha = (2m_b + Nm_c)g\sin\alpha \tag{35}$$

which shows that the minimum acceleration needed to initiate uplift of a rocking frame is

$$\ddot{u}_g^{up} = g\tan\alpha \tag{36}$$

According to equation (36), the minimum uplift acceleration of the rocking frame depends solely on the slenderness of its columns and is entirely independent of the mass of the cap beam (epistyles and frieze atop). This result was expected from the previous analysis on the rocking motion of the free-standing frame (see equation 26), which showed that its dynamic rocking response is identical to the rocking responseof a single column that has the same slenderness, α, as the columns of the rocking frame, but larger size, $\hat{R} = ((1 + 3\gamma)/(1 + 2\gamma))R$ (see Figure 6).

5. MAXIMUM COEFFICIENT OF RESTITUTION

The maximum coefficient of restitution of the rocking frame during the impact that happens when the rotation $\theta(t)$ alternates sign is calculated by applying the angular momentum-impulse theorem on one column of the frame before and after the impact. As in the case of the solitary rocking column, the angular momentum of one column of the rocking frame with respect to the imminent pivot point O′ (see Figure 7) is

$$H_1 = (I_o - 2m_c bR\sin\alpha)\dot{\theta}_1, \tag{37}$$

where $\dot{\theta}_1$ is the angular velocity of the rocking column just before the impact. Upon impact, the angular momentum of the column with respect to the new pivot point O′ is

$$H_2 = I_o\dot{\theta}_2 \tag{38}$$

where $\dot{\theta}_2$ is the angular velocity of the rocking column immediately after the impact.

The main difference between the conservation of angular momentum before and after the impact of the free-standing rocking frame with a freely supported cap beam and the rocking of a free-standing solitary column is that upon impact happens, additional forces are acting on the columns of the rocking frame that were absent in the solitary column. These forces appear when the reactions of the cap beam (epistyle) shift from point P′ to point P as the pivot points at the base shift from point O to O′ (see Figure 7)

DOI: 10.1002/eqe

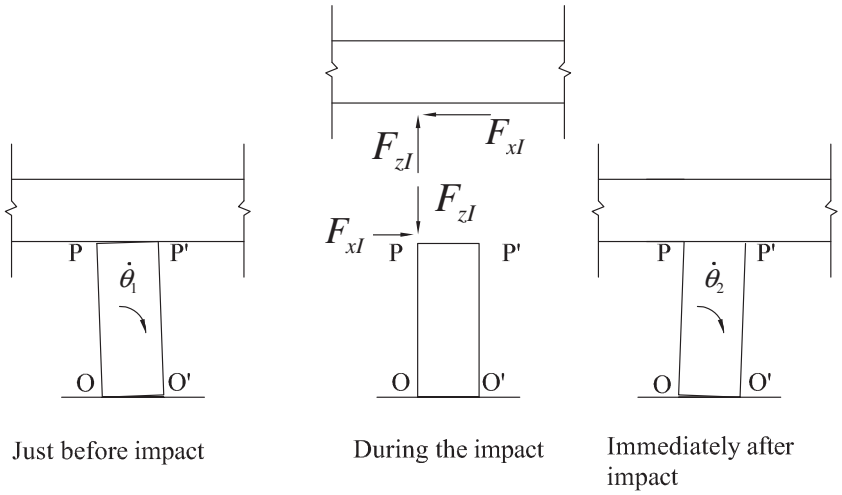

Figure 7. Configuration of the rocking column of the free-standing frame just before and immediately after the impact together with the impact forces that develop at point P as the pivoting transfers to point O′.

Given that the cap beam is rigid and that during the rocking motion of the frame, the motion of the cap beam is only a translation (no rotations), it is assumed that the impact forces at all columns are equal. Accordingly, the change of the linear momentum of the cap beam in the horizontal and vertical directions before and after the impact is

$$N \int_{\substack{\text{duration}\\ \text{of impact}}} F_{xI}\mathrm{d}t = 2m_b R\cos\alpha\left(\dot{\theta}_1 - \dot{\theta}_2\right) \tag{39}$$

and

$$N \int_{\substack{\text{duration}\\ \text{of impact}}} F_{zI}\mathrm{d}t = 2m_b R\sin\alpha\left(\dot{\theta}_1 + \dot{\theta}_2\right) \tag{40}$$

Application of the angular momentum – impulse theorem before and after the impact – gives

$$H_1 - 2b \int_{\substack{\text{duration}\\ \text{of impact}}} F_{zI}\mathrm{d}t + 2h \int_{\substack{\text{duration}\\ \text{of impact}}} F_{xI}\mathrm{d}t = H_2 \tag{41}$$

After substituting equation (37)–(40) into eqaution (41) and using that $I_o = 4/3m_cR^2$, one obtains

$$\left(\frac{4}{3}m_c - 2m_c\sin^2\alpha - \frac{4}{N}m_b\sin^2\alpha + \frac{4}{N}m_b\cos^2\alpha\right)\dot{\theta}_1 = \left(\frac{4}{N}m_b + \frac{4}{3}m_c\right)\dot{\theta}_2 \tag{42}$$

Further simplification of equation (42) gives that the ratio of kinetic energy of the rocking frame after and before the impact is

DOI: 10.1002/eqe

$$r = \left(\frac{\dot{\theta}_2}{\dot{\theta}_1}\right)^2 = \left(\frac{1 - \frac{3}{2}\sin^2\alpha + 3\gamma\cos 2a}{1 + 3\gamma}\right)^2 \tag{43}$$

Equation (43) indicates that the angular velocity of the rocking frame after the impact is only $\sqrt{r}$ times the velocity before the impact. Figure 8 plots the value of the minimum coefficient of restitution $\sqrt{r} = \left(1 - (3/2)\sin^2\alpha + 3\gamma\cos 2a\right)/(1 + 3\gamma)$ as a function of the slenderness α for different values of the mass ratio $\gamma = m_b/Nm_c$.

Figure 8 indicates that the maximum coefficient of restitution $\sqrt{r}$ of the rocking frame is always smaller than the maximum coefficient of restitution of the solitary column $= 1 - (3/2)\sin^2\alpha$, indicating that when a free-standing frame engages into rocking motion, it dissipates more energy than the equal slenderness equivalent solitary free-standing column with size $\hat{R}$ because of the additional impacts that happen between the columns and the cap beam (epistyles and frieze).

6. OVERTURNING SPECTRA – SELF-SIMILAR RESPONSE FOR PULSE-LIKE EXCITATIONS

The relative simple form yet destructive potential of near source ground motions has motivated the development of various closed form expressions that approximate their dominant kinematic characteristics. The early work of Veletsos *et al*. [17] was followed by the papers of Hall *et al*. [18], Makris [19], Makris and Chang [20], Alavi and Krawinkler [21], and more recently by the papers of Mavroeidis and Papageorgiou [22] and Vassiliou and Makris [23]. Physically realizable pulses can adequately describe the impulsive character of near-fault ground motions both qualitatively and quantitatively. The minimum number of parameters of the mathematical pulse is two, which are the acceleration amplitude, a_p, and the duration, T_p. The more sophisticated model of Mavroeidis and Papageorgiou [22] involves four parameters: the pulse period, the pulse amplitude, the pulse phase, and the number of half cycles. Recently, Vassiliou and Makris [23] used the Mavroeidis and Papageorgiou model [22] in association with wavelet analysis to develop a mathematically formal and objective procedure to extract the time scale and length scale of strong ground motions.

The current established methodologies for estimating the pulse characteristics of a wide class of records are of unique value because the product, $a_p T_p^2 = L_p$, is a characteristic length scale of the ground excitation and is a measure of the persistence of the most energetic pulse to generate inelastic deformation [24, 25]. It is emphasized that the persistence of the pulse, $a_p T_p^2 = L_p$, is a different characteristic than the strength of the pulse that is measured with the peak pulse acceleration, a_p. The reader may recall that among two pulses with different acceleration amplitudes (say $a_{p1} > a_{p2}$) and different pulse durations (say $T_{p1} < T_{p2}$), the inelastic deformation does not scale

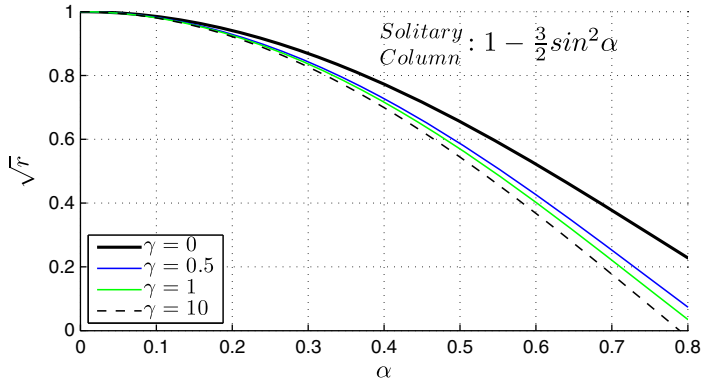

Figure 8. Values of the maximum coefficient of restitution as a function of the slenderness, α of the columns of the rocking frame for different values of the mass ratio $\gamma = m_b/Nm_c$.

DOI: 10.1002/eqe

with the peak pulse acceleration (most intense pulse) but with the strongest length scale (larger $a_{\mathrm{p}}T_{\mathrm{p}}{}^{2}$ = most persistent pulse) [24–26].

The heavy dark line in Figure 9 (Top) that approximates the long-period acceleration pulse of the NS component of the 1992 Erzincan, Turkey, record is a scaled expression of the second derivative of the Gaussian distribution, $e^{-t^2/2}$, known in the seismological literature as the symmetric Ricker wavelet [27, 28]

$$\psi(t) = a_p \left(1 - \frac{2\pi^2 t^2}{T_p^2}\right) e^{-\frac{12\pi^2 t^2}{2\ T_p^2}} \tag{44}$$

The value of $T_p = 2\pi/\omega_p$ is the period that maximizes the Fourier spectrum of the symmetric Ricker wavelet. Similarly, the heavy dark line in Figure 9 (Bottom), which approximates the long-period acceleration pulse of the Pacoima Dam motion recorded during the 9 February 1971 San Fernando, California earthquake, is a scaled expression of the third derivative of the Gaussian distribution $e^{-t^2/2}$.

$$\psi(t) = \frac{a_p}{\beta}\left(\frac{4\pi^2 t^2}{3T_p^2} - 3\right) t e^{-\frac{14\pi^2 t^2}{2\ 3T_p^2}} \tag{45}$$

in which β is a factor equal to 1.3801 that enforces the aforementioned function to have a maximum equal to a_{p}.

The choice of the specific functional expression to approximate the main pulse of pulse-type ground motions has limited significance in this work. What is important to recognize is that several strong

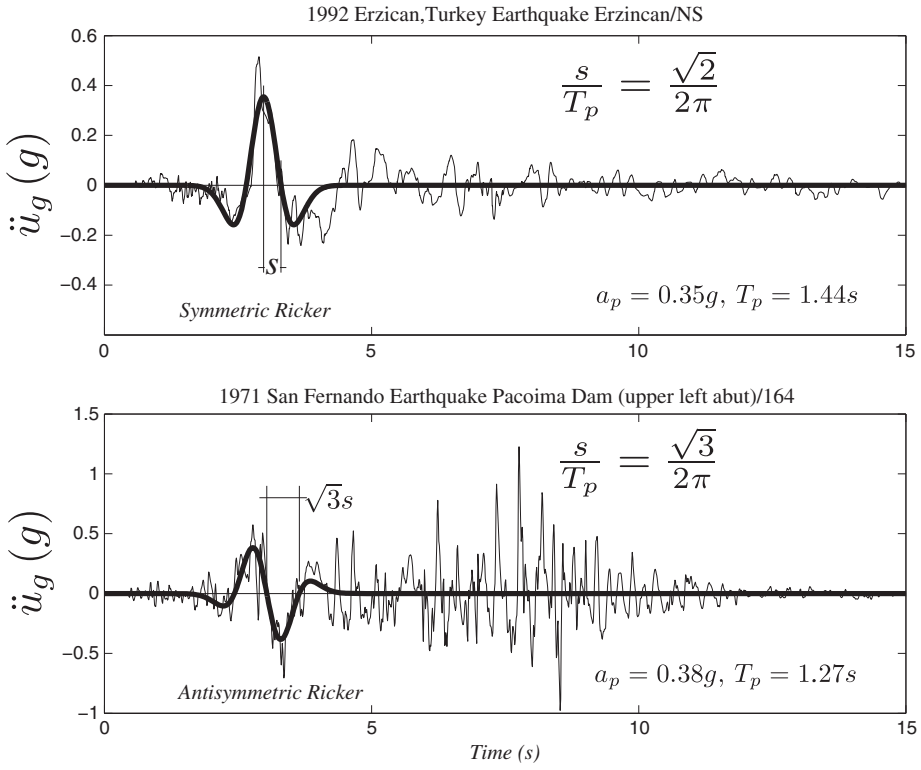

Figure 9. Top: north–south components of the acceleration time history recorded during the 1992 Erzican, Turkey earthquake together with a symmetric Ricker wavelet. Bottom: fault-normal component of the acceleration time history recorded during the 1971 San Fernando earthquake, together with an antisymmetric Ricker wavelet.

DOI: 10.1002/eqe

ground motions contain a distinguishable acceleration pulse that is responsible for most of the inelastic deformation of structures ([18, 20, 21, 29, 24] among others). A mathematically rigorous and easily reproducible methodology based on wavelet analysis to construct the best matching wavelet has been recently proposed by Vassiliou and Makris [23].

Consider the free-standing rocking frame shown in Figure 1 that is subjected to an acceleration pulse (like those shown in Figure 9) with acceleration amplitude a_{p} and pulse duration, $T_p = 2\pi/\omega_p$. From equation (26), it results that the response of a free-standing rocking frame subjected to an acceleration pulse is a function of six variables

$$\theta(t) = f\left(p, \alpha, \gamma, g, a_p, \omega_p\right) \tag{46}$$

The seven variables appearing in equation (46) involve only two reference dimensions; that of length [L] and time [T]. According to Buckingham's Π theorem, the number of dimensionless products with which the problem can be completely described is equal to [number of variables = 7] − [number of reference dimensions = 2] = 5. Herein, we select as repeating variables the characteristics of the pulse excitation, a_{p} and ω_{p}, and the five independent Π products as follows: $\Pi_\theta = \theta$, $\Pi_\omega = \omega_{\mathrm{p}}/p$, $\Pi_\alpha = \tan\alpha$, $\Pi_\gamma = \gamma$, and $\Pi_{\mathrm{g}} = a_{\mathrm{p}}/g$. With these five dimensionless Π products, equation (46) reduces to

$$\theta(t) = \varphi\left(\frac{\omega_p}{p}, \tan\alpha, \gamma, \frac{a_p}{g}\right) \tag{47}$$

The rocking response of the free-standing frame shown in Figure 1 when subjected to a horizontal base acceleration history $\ddot{u}_g(t)1/2$ is computed by solving equation (26) in association with the minimum energy loss expression given by equation (43) that takes place at every impact.

Figure 10 shows the minimum overturning acceleration spectra of a free-standing rocking frame when subjected to a symmetric Ricker pulse (left) and an antisymmetric Ricker pulse (right) for different values of the mass ratio $\gamma = m_b/Nm_c$. The top plots are for values of the column slenderness $\alpha = 10^\circ$ and the bottom plots are for $\alpha = 14^\circ$.

In constructing Figure 10, the frequency parameter p is the frequency parameter of the columns of the frame (not $\hat{p}$) and the enhanced stability of the rocking frame due to (i) the corresponding larger size, $\hat{p} = \sqrt{(1+2\gamma)/(1+3\gamma)}p$, and (ii) the reduced coefficient of restitution (see equation (43)) is given by the curves for each given value of γ.

Figure 10 indicates that up to values of $\omega_{\mathrm{p}}/p = 4$, the additional stability of the rocking frame versus the stability of the equal slenderness solitary column is marginal.

For values of $\omega_{\mathrm{p}}/p > 4$ (larger columns or shorter period pulses), the minimum acceleration overturning spectra of the rocking frame are higher than the corresponding spectrum of the solitary rocking column showing the enhanced seismic stability of the top-heavy rocking frame. This enhanced seismic stability is indifferent to the height of the center of gravity of the cap beam.

7. SEISMIC STABILITY OF ANCIENT COLUMNS SUPPORTING EPISTYLES AND THE FRIEZE ATOP

In ancient Greek temples, the epistyles are positioned from the vertical axis of one column to the vertical axis of the neighboring column; therefore, the joint of the epistyles are along the vertical axis of the column (see Figure 2). With this configuration during lateral loading of the peristyle of the temple, each epistyle in addition to the horizontal translation, u, shown in Figure 1 will also experience a small rotation, whereas the transfer of forces from the epistyles to the columns is not concentrated at the top pivoting point of the columns. During a planar lateral motion of the peristyle, the tendency of the epistyle to rotate is partially prevented from the friction that develops along the interface with the neighboring high-profile epistyle and the heavy stone of the frieze atop

DOI: 10.1002/eqe

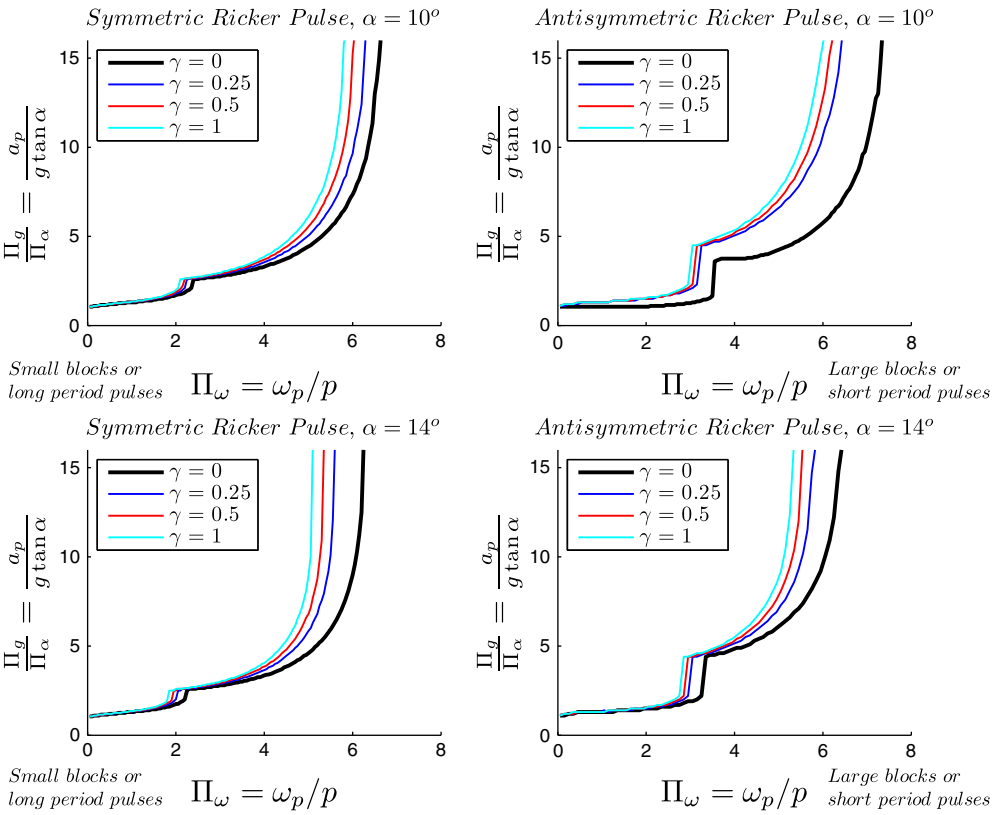

Figure 10. Minimum overturning acceleration spectra of the free-standing rocking frame shown in Figure 1 when subjected to a symmetric Ricker pulse (left) and an antisymmetric Ricker pulse (right) for different values of the mass ratio $\gamma = m_b/Nm_c$. Top: $\alpha = 10°$; bottom: $\alpha = 14°$. The values of the coefficient of restitution are given by equation (43).

that goes over the joint of the epistyles. According to this construction pattern with very tight joints that 'lock' the stones, the ancient builders constructed a nearly continuous and massive structure atop the columns, which according to this study enhanced appreciably the seismic-rocking stability of the peristyle of the temples. It is worth mentioning that the numerical study of Papaloizou and Komodromos [16], which accounts for the individual motion of each epistyle without supporting a frieze atop, concludes to the same result – that the planar response of free-standing rocking frames is more stable than the response of their solitary free-standing columns.

Two of the strongest ground motions recorded in Greece are the 1973 Lefkada record and the 1995 Aigion record [23]. Both records exhibit distinguishable acceleration pulses with durations $T_p \approx 0.6$ s. We concentrate on the Temple of Apollo in Corinth where its 7.5 m × 1.8 m monolithic columns remain standing since 540 BC in an area with high seismicity. The dimensions of its columns yield a frequency parameter $p = \sqrt{3g/4R} = 1.4\ rad/s$ and a slenderness $\alpha = \tan^{-1}(b/h) = 13.5°$. By taking the pulse duration $T_p = 0.6$ s of the nearby Aigion record, the dimensionless term Π_ω assumes the value $\omega_p/p = 2\pi/pT_p = 7.5$. For such large value of $\omega_p/p \approx 7.5$, the bottom plots of Figure 10 give for the solitary free-standing column ($\gamma = 0$ line) an overturning ground acceleration $a_p > 15\, g \tan\alpha = 15\, g \times 0.24 = 3.6\, g$, which is an unrealistically high acceleration. Consider now the extreme situation for Greece, where the predominant pulse of the ground shaking exhibits a period $T_p = 0.9$ s. A pulse period $T_p = 0.9$ s may be a rare event for the fault size and earthquake magnitude that prevail in Greece; nevertheless, it helps one understanding the appreciable seismic stability of rocking structures.

With $T_p = 0.9$ s and $p = 1.4$ rad/s, $\omega_p/p = 5$, and according to the bottom plots of Figure 10, which are for slenderness $\alpha = 14°$, the minimum overturning acceleration of a rocking frame with $\gamma = 0.25$ exceeds the value of $a_p \approx 5\, g \times 0.24 = 1.2\, g$. This analysis shows that the free-standing peristyles of

DOI: 10.1002/eqe

ancient temples can survive acceleration pulses as long as 0.9 s and as intense as 1.2 g. Although this is a physically realizable pulse [30], it is an unlikely strong shaking for the seismicity of Greece that apparently never happened over the 2500 years of the lifespan of the temples shown in Figures 2 and 3.

8. ROCKING ISOLATION OF BRIDGES – PROOF OF CONCEPT

The concept of allowing the piers of bridges to rock is not new. For instance, the beneficial effects that derive from uplifting and rocking have been implemented since the early 1970s in the South Rangitikei bridge in New Zealand [31]. During the last decade, the benefits/challenges associated with the rocking of bridge piers have been receiving increasing attention partly because of growing interest in the prefabricated bridge technology ([32–34] and the references reported therein) and partly because of the need for the bridge structure to re-center after a strong seismic event ([35, 36] among others).

In the prefabricated bridge technology, the bridge piers and the deck are not free standing. The structural system is essentially a hybrid system (see [32, 36]) where the bridge pier is connected to its foundation and at the deck with a post-tensioned tendon that passes through the axis of the column together with longitudinal mild-steel reinforcement that runs near the circumference of the column. During earthquake loading, the majority of deformation is concentrated at the pier-foundation and pier-cap beam interfaces, and the overall deformation pattern of the post-tensioned pier-cap beam system resembles the deformation pattern of the free-standing rocking frame that is under investigation in this study. Nevertheless, the post-tensioning tendons and the mild-steel longitudinal reinforcement that extends into the foundation and the cap beam contributes appreciably to the lateral moment capacity of the system, and in most prefabricated bridge applications, the moment–rotation curve of the hybrid systems follows a positive slope.

Within the context of a proof of concept, in this study, we present the planar rocking response of a free-standing two-column bridge bent where its moment–rotation curve follows a negative slope given that the frame is entirely free to rock (see Figure 5). Figure 11 shows schematically the free-standing two-column bridge bent of interest in its deformed configuration. Sliding at the pivot point during impact is prevented with a recess at the pile cap and the cap beam as shown in Figure 11. In this numerical application, the cylindrical piers of the free-standing bridge bent are 9.6-m tall with a diameter $d = 2b = 1.6$ m. These are typical dimensions of bridge piers for highway overpasses and other bridges in Europe and USA. Taller bridge piers will result to even more stable configurations. With $2h = 9.6$ m and $2b = 1.6$ m, the slenderness of the bridge pier is $\tan\alpha = 1/6 = 0.166$, and its frequency parameter $p = 1.23$.

Depending on the length of the adjacent spans and the per-length weight of the deck, the mass ratio $\gamma = m_b/2m_c$ assumes values from 4 and above ($\gamma > 4$). The larger the value of γ (heavier deck), the more

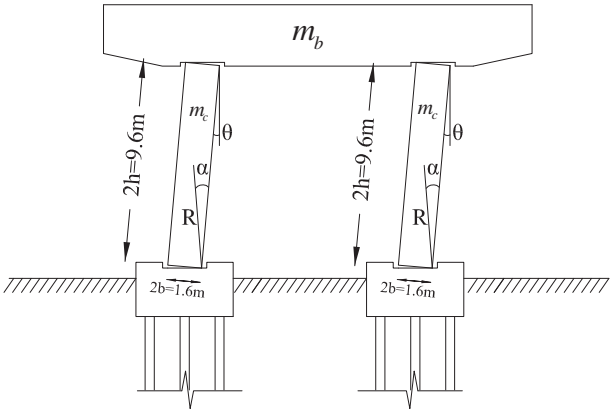

Figure 11. Free-standing rocking bridge bent. Potential sliding during impact is prevented with the recess shown. No vertical post-tensioning, no continuation of the longitudinal reinforcement of the columns through the rocking interfaces at the pile caps and the cap beam.

DOI: 10.1002/eqe

stable is the free-standing rocking frame (see Figure 10). The seismic response analysis of the rocking frame has been studied until this section by using ground excitation acceleration; that is, pulses described either by symmetric or antisymmetric Ricker wavelets. The acceleration amplitude, a_p, and the duration, T_p, of any distinct acceleration pulse allow the use of the dimensional analysis presented in this work and the derivation of the associated Π products that improve the understanding of the physics that govern the problem together with the organization and presentation of the response. Nevertheless, to stress the main finding of this study – that top-heavy free-standing rocking frames enjoy ample seismic stability – we examine the planar seismic response of the free-standing two-column bridge bent shown in Figure 11 when subjected to six strong-motion historic records listed in Table I. The values of the acceleration amplitude, a_p, and pulse period, T_p, shown in last two columns of Table I have been determined with the extended wavelet transform [23].

Figure 12 plots the time histories of the normalized rotation, θ/α, together with the vertical uplift, $v(t)$, and the horizontal drift, $u(t)$, of the free-standing rocking bridge bent shown in Figure 11 with $\gamma = m_b/2m_c = 4$. Note that for all six strong ground motions selected in this analysis, the frame rotation, θ, is less than 1/3 of the slenderness, α, of the columns ($\theta/\alpha < 0.33$); therefore, the free-standing rocking frame exhibits ample seismic stability.

The peak horizontal displacement u_{max} ranges from 20 to 50 cm; whereas the vertical uplift is as high as 5 cm. The evaluation of these response quantities shall be conducted in association with the equivalent response quantities from vertically post-tensioned hybrid frames [32, 33, 36] and seismically isolated decks ([37–39] among others) after considering the effects of the end-conditions of the deck at the abutments. This comparison/evaluation is the subject of an ongoing study that also examines other practical issues such as the effect of the crushing of the pivoting points of the columns [40, 41] and the accommodation of the deck uplift at the end-abutments.

The main conclusion of this study is that heavy decks freely supported on free-standing piers exhibit ample seismic stability and that the heavier is the deck (even if the center of gravity rises), the more stable is the rocking frame. This conclusion may eventually lead to the implementation of the free-standing rocking frame – a structural configuration where all the issues associated with seismic connections such as buckling and fracture of the longitudinal reinforcing bars or spalling of the concrete cover [32–36] are removed as they are not an issue in the ancient temples shown in Figures 2 and 3.

9. CONCLUSIONS

This paper investigated the planar rocking response of an array of free-standing columns capped with a freely supported rigid beam. Following a variational formulation, the paper concludes to the remarkable result that the planar dynamic rocking response of an array of free-standing columns capped with a rigid beam is identical to the rocking response of a single free-standing column with the same slenderness as the slenderness of the columns of the rocking frame yet with larger size and more energy loss during impacts. A larger size rocking column corresponds to a more stable configuration; therefore, the presence of the freely supported cap beam renders the rocking frame more stable despite the rise of the center of gravity.

Table I. Earthquake records used for the seismic response analysis of the free-standing rocking bridge bent.

Earthquake	Record	Magnitude (Mw)	Epicentral distance (km)	PGA (g)	PGV (m/s)	a_p (g)	T_p (s)
1966 Parkfield	CO2/065	6.1	0.1	0.48	0.75	0.41	0.6
1971 San Fernando	Pacoima Dam/164	6.6	11.9	1.23	1.13	0.38	1.27
1986 San Salvador	Geotech Investigation Center	5.4	4.3	0.48	0.48	0.34	0.8
1992 Erzican,	Erzincan/EW	6.9	13	0.50	0.64	0.34	0.9
1994 Northridge	Jensen Filter Plant/022	6.7	6.2	0.57	0.76	0.39	0.5
1995Kobe	Takarazuka/000	6.9	1.2	0.69	0.69	0.50	1.1

DOI: 10.1002/eqe

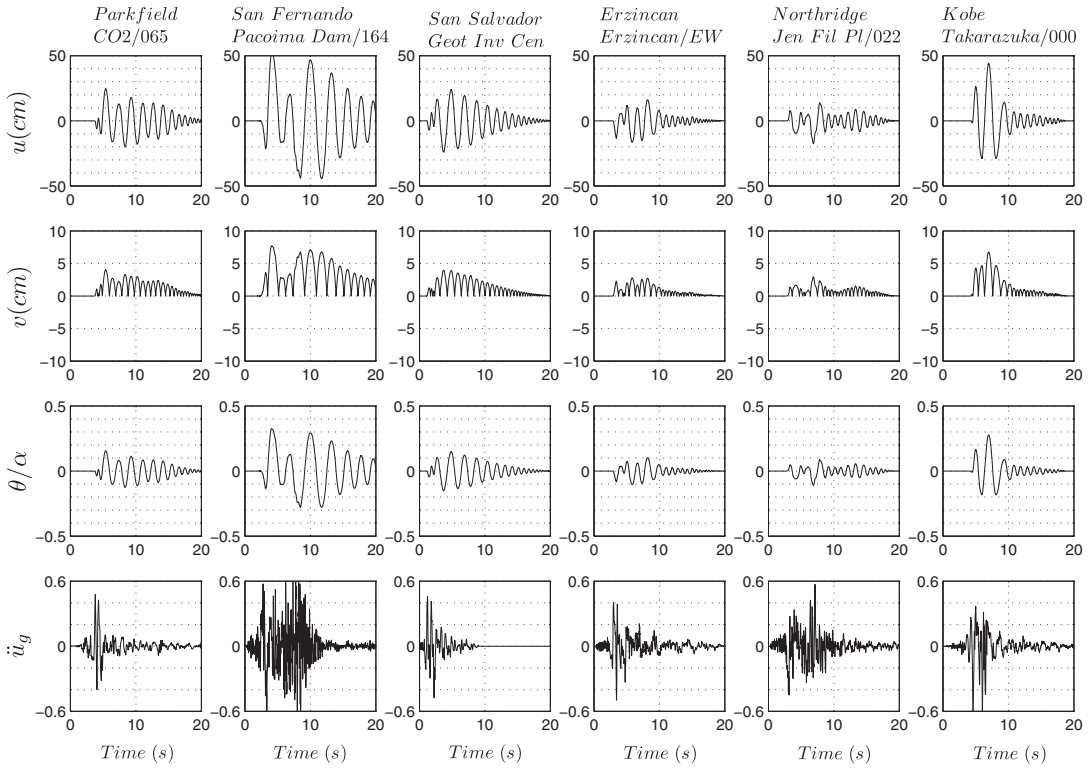

Figure 12. Rotation, vertical, and horizontal displacement histories of the free-standing rocking frame shown in Figure 11 ($p = 1.23$, $\tan\alpha = 1/6$, $\gamma = 4$) when subjected to the recorded ground motions listed in Table I and plotted at the bottom.

Most importantly, the study shows that the heavier the freely supported cap beam is, the more stable is the rocking frame implying that top-heavy rocking frames are more stable than when they are top light. The stability of the rocking frame is independent of the number of columns and depends only on the ratio of the weight that is transferred to the column to the weight of the column together with the size and the slenderness of the columns.

The acceleration needed to create uplift of the rocking frame is independent of the mass and the height of the center of gravity of the cap beam and depends only on the slenderness, α, of the columns ($u_g^{up} = g\tan\alpha$).

The aforementioned findings render rocking isolation a most attractive alternative for the seismic protection of bridges given that the heavier is the deck, the more stable is the rocking bridge. The future implementation of a truly rocking frame where there is neither post-tensioning nor continuation of the longitudinal reinforcement through the rocking interfaces shall remove several of the concerns associated with the seismic connections of prefabricated bridges such as buckling and fracture of the longitudinal reinforcing bars or spalling of the concrete cover.

ACKNOWLEDGEMENTS

Financial support for this study has been provided by the project 'Aristeia' that is implemented under the NSRF – 'OPERATIONAL PROGRAMME EDUCATION AND LIFELONG LEARNING' and is co-funded by the European Union (European Social Fund) and the Greek State (Ministry of Education, Lifelong Learning and Religious Affairs – Greek General Secretariat for Research and Technology).

REFERENCES

1. Milne J. Seismic experiments. *Transactions of the Seismological Society of Japan* 1885; **8**:1–82.
2. Housner GW. The behaviour of inverted pendulum structures during earthquakes. *Bulletin of the Seismological Society of America* 1963; **53**(2):404–417.

DOI: 10.1002/eqe

3. Yim CS, Chopra AK, Penzien J. Rocking response of rigid blocks to earthquakes. *Earthquake Engineering and Structural Dynamics* 1980; **8**(6):565–587.
4. Aslam M, Scalise DT, Godden WG. Earthquake rocking response of rigid blocks. *Journal of the Structural Engineering Division (ASCE)* 1980; **106**(2):377–392.
5. Psycharis IN, Jennings PC. Rocking of slender rigid bodies allowed to uplift. *Earthquake Engineering and Structural Dynamics* 1983; **11**:57–76. DOI: 10.1002/eqe.4290110106
6. Spanos PD, Koh AS. Rocking of rigid blocks due to harmonic shaking. *Journal of Engineering Mechanics* (ASCE) 1984; **110**(11):1627–1642.
7. Hogan SJ. On the dynamics of rigid-block motion under harmonic forcing. *Proceedings of the Royal Society of London* 1989; **A425**:441–476.
8. Hogan SJ. The many steady state responses of a rigid block under harmonic forcing. *Earthquake Engineering and Structural Dynamics* 1990; **19**(7):1057–1071.
9. Zhang J, Makris N. Rocking response of free-standing blocks under cycloidal pulses. *Journal of Engineering Mechanics* (ASCE) 2001; **127**(5):473–483.
10. Makris N, Konstantinidis D. The rocking spectrum and the limitations of practical design methodologies. *Earthquake Engineering and Structural Dynamics* 2003; **32**:265–289.
11. Prieto F, Lourenço PB, Oliveira CS. Impulsive Dirac-delta forces in the rocking motion. *Earthquake Engineering and Structural Dynamics* 2004; **33**:839–857. DOI: 10.1002/eqe.381
12. Apostolou M, Gazetas G, Garini E. Seismic response of slender rigid structures with foundation uplift. *Soil Dynamics and Earthquake Engineering* 2007; **27**:642–654
13. Palmeri A, Makris N. Response analysis of rigid structures rocking on viscoelastic foundation. *Earthquake Engineering and Structural Dynamics* 2008; **37**: 1039–1063. DOI: 10.1002/eqe.800
14. Vassiliou MF, Makris N. Analysis of the rocking response of rigid blocks standing free on a seismically isolated base. *Earthquake Engineering and Structural Dynamics* 2011. DOI: 10.1002/eqe.1124
15. Makris N, Roussos Y. Rocking response of rigid blocks under near-source ground motions. *Geotechnique* 2000; **50**(3):243–262.
16. Papaloizou L, Komodromos K. Planar investigation of the seismic response of ancient columns and colonnades with epistyles using a custom-made software. *Soil Dynamics and Earthquake Engineering* 2009; **29**(11–12): 1437–1454.
17. Veletsos AS, Newmark NM, Chelepati CV. Deformation spectra for elastic and elastoplastic systems subjected to ground shock and earthquake motions. *Proceedings of the 3rd World Conference on Earthquake Engineering*, vol. II, Wellington, New Zealand, 1965; 663–682.
18. Hall JF, Heaton TH, Halling MW, Wald DJ. Near-source ground motion and its effects on flexible buildings. *Earthquake Spectra* 1995; **11**(4):569–605.
19. Makris N. Rigidity–plasticity–viscosity: can electrorheological dampers protect base-isolated structures from near-source ground motions? *Earthquake Engineering and Structural Dynamics* 1997; **26**:571–591.
20. Makris N, Chang S-P. Effect of viscous, viscoplastic and friction damping on the response of seismic isolated structures. *Earthquake Engineering and Structural Dynamics* 2000; **29**(1):85–107.
21. Alavi B, Krawinkler H. Effects of near-source ground motions on frame-structures. *Technical Report No. 138*, The John A. Blume Earthquake Engineering Center, Stanford University, 2001.
22. Mavroeidis GP, Papageorgiou AS. A mathematical representation of near-fault ground motions. *Bulletin of the Seismological Society of America* 2003; **93**(3):1099–1131.
23. Vassiliou MF, Makris N. Estimating time scales and length scales in pulse-like earthquake acceleration records with wavelet analysis. *Bulletin of the Seismological Society of America* 2011; **101**(2): 596–618.
24. Makris N, Black CJ. Dimensional analysis of rigid-plastic and elastoplastic structures under pulse-type excitations. *Journal of Engineering Mechanics* (ASCE) 2004; **130**(9):1006–1018.
25. Makris N, Black CJ. Dimensional analysis of bilinear oscillators under pulse-type excitations. *Journal of Engineering Mechanics* (ASCE) 2004; **130**(9):1019–1031.
26. Karavasilis TL, Makris N, Bazeos N, Beskos DE. Dimensional response analysis of multistory regular steel MRF subjected to pulselike earthquake ground motions. *Journal of Structural Engineering* 2010; **136**(8): 921–932.
27. Ricker N. Further developments in the wavelet theory of seismogram structure. *Bulletin of the Seismological Society of America* 1943; **33**:197–228.
28. Ricker N. Wavelet functions and their polynomials. *Geophysics* 1944; **9**:314–323.
29. Makris N, Psychogios C. Dimensional response analysis of yielding structures with first-mode dominated response. *Earthquake Engineering and Structural Dynamics* 2006; **35**:1203–1224
30. Loh C-H, Lee Z-K, Wu T-C, Peng S-Y. Ground motion characteristics of the Chi-Chi earthquake of 21 September 1999. *Earthquake Engineering and Structural Dynamics* 2000; **29**:867–897.
31. Beck JL, Skinner RI. The seismic response of a reinforced concrete bridge pier designed to step. *Earthquake Engineering and Structural Dynamics* 1974; **2**:343–358.
32. Wacker JM, Hieber DG, Stanton JF, Eberhard MO. Design of precast concrete piers for rapid bridge construction in seismic regions. *Research Report*, Federal Highway Administration, 2005.
33. Pang JBK, Stenk KP, Cohagen L, Stanton JF, Eberhard MO. Rapidly constructible large-bar precast bridge-bent seismic connection. *Research Report WA-RD684.2*, Washington State Department of Transportation, 2008.

DOI: 10.1002/eqe

34. Cohagen L, Pang JBK, Stanton JF, Eberhard MO. A precast concrete bridge bent designed to recenter after an earthquake. *Research Report*, Federal Highway Administration, 2008.
35. Sakai J, Hyungil J, Mahin S. Reinforced concrete bridge columns that re-center following earthquakes. *Proceedings of the 8th US National Conference on Earthquake Engineering*, San Francisco, California, USA, April 18–22, 2006.
36. Cheng CT. Shaking table tests of a self-centering designed bridge substructure. *Engineering Structures* 2008; **30**:3426–3433.
37. Constantinou MC, Soong TT, Dargush GF. Passive energy dissipation Systems for Structural Design and Retrofit. *Monograph Series*, MCEER, University of Buffalo, NY, 1998.
38. Makris N, Zhang J. Seismic response analysis of highway overcrossings equipped with elastomeric bearings and fluid dampers. *Journal of Structural Engineering* (ASCE) 2004; **130**(6):830–845.
39. Buckle IG, Constantinou MC, Diclali M, Chasemi H. Seismic isolation of highway bridges. *Research Report MCEER-06-SP07*, MCEER, University of Buffalo, NY, 2006.
40. Roh H, Reinhorn A. Nonlinear static analysis of structures with rocking columns. *Journal of Structural Engineering* (ASCE) 2010; **136**(5):532–542.
41. Roh H, Reinhorn A. Modeling and seismic response of structures with concrete rocking columns and viscous dampers. *Engineering Structures* 2010; **32**(8):2096–2107.

DOI: 10.1002/eqe